

OPEN

Developing a xenograft model of human vasculature in the mouse ear pinna

Gavin R. Meehan¹, Hannah E. Scales¹, Rowland Osii¹, Mariana De Niz^{1,3}, Jennifer C. Lawton¹, Matthias Marti¹, Paul Garside¹, Alister Craig² & James M. Brewer^{1*}

Humanised xenograft models allow for the analysis of human tissue within a physiological environment *in vivo*. However, current models often rely on the angiogenesis and ingrowth of recipient vasculature to perfuse tissues, preventing analysis of biological processes and diseases involving human blood vessels. This limits the effectiveness of xenografts in replicating human physiology and may lead to issues with translating findings into human research. We have designed a xenograft model of human vasculature to address this issue. Human subcutaneous fat was cultured *in vitro* to promote blood vessel outgrowth prior to implantation into immunocompromised mice. We demonstrate that implants survived, retained human vasculature and anastomosed with the circulatory system of the recipient mouse. Significantly, by performing transplants into the ear pinna, this system enabled intravital observation of xenografts by multiphoton microscopy, allowing us to visualise the steps leading to vascular cytoadherence of erythrocytes infected with the human parasite *Plasmodium falciparum*. This model represents a useful tool for imaging the interactions that occur within human tissues *in vivo* and permits visualization of blood flow and cellular recruitment in a system which is amenable to intervention for various studies in basic biology together with drug evaluation and mechanism of action studies.

Xenograft models, in which human cells, tissues or organs are implanted into immunodeficient animal hosts have proven to be valuable research tools in recent years^{1,2}. By allowing human tissue to be studied in an *in vivo* environment, these models provide a physiologically relevant method for assessing human diseases that neither conventional animal models nor human *in vitro* studies are able to achieve alone.

A wide array of tissues have been examined in these models including hematopoietic stem cells, liver and thymus fragments³, adipose tissue⁴, testicular tissue⁵, tumours⁶ and even human brain organoids⁷. However, the majority of xenografts tend to consist of cells or small organoids as a major challenge of using tissue fragments is the re-establishment of blood flow to the grafts. When a tissue is first implanted into an animal, cells within a distance of 150–200 µm of a blood vessel survive through molecular diffusion but those cells deeper in the graft experience hypoxia and glucose deprivation⁸. This triggers the release of soluble mediators including vascular endothelial growth factor (VEGF) which induce both host and graft endothelial cells (ECs) to initiate angiogenesis⁹. This allows the ECs to self-replicate and form hollow capillary sprouts that continue to grow until they meet and connect with another capillary, resulting in the restoration of normal blood flow.

During this process of neovascularisation, the vessels from the host tend to grow into the graft in a process known as internal inosculation. This results in a substantial proportion of the graft vasculature originating from the host, and a loss of the vasculature of graft origin^{10,11}, limiting the ability to effectively study the function of human vasculature within human xenografts¹².

Research in a variety of areas would benefit from a xenograft system that would allow non-invasive *in vivo* visualisation of cellular interactions occurring within and around human vasculature. These include research examining vascular remodelling and repair, models of acute inflammation as well as various infection studies examining the interactions of bacteria or protozoan parasites with human tissue¹³. A model allowing for the visualisation of the vascular cytoadherence of *Plasmodium falciparum* would be particularly useful, as this process

¹Institute of Infection, Immunity & Inflammation, University of Glasgow, Scotland, UK. ²Liverpool School of Tropical Medicine, Liverpool, UK. ³Instituto de Medicina Molecular, University of Lisbon, Lisbon, Portugal. *email: james.brewer@glasgow.ac.uk

is thought to be a major contributor to a deadly form of disease¹⁴, known as cerebral malaria, but cannot be replicated in murine malaria models.

Accordingly, we designed a new model that incorporated human tissue in a site that was minimally invasive and allowed for longitudinal imaging: the ear pinna. We demonstrated that by pre-culturing the tissue prior to implantation we could promote the retention of human vasculature and the successful re-perfusion of the graft. Using the human specific parasite *P. falciparum*, we validated the function of the model and visualised binding of the parasite to the endothelium.

Methods

Mice. NOD SCID Gamma mice (NSG)¹⁵ (originally purchased from Jackson Laboratories, Bar Harbor, ME, USA) were produced in house (Central Research Facility, University of Glasgow, UK). These mice were bred in a sterile film isolator and maintained in individually ventilated cages (IVC). Animals were maintained on a 12-hour light/dark cycle and provided with food and water *ad libitum*. All procedures were performed under a UK Home Office licence in accordance with the Animals (Scientific Procedures) Act 1986.

Ethical approval. The use of human tissue within this study was approved by the NHS Greater Glasgow and Clyde Biorepository (application number 97) on behalf of the NHS Research Ethics Committee. Informed consent was obtained from all subjects. All tissue was processed in accordance with the Human Tissue (Scotland) Act 2006.

Human tissue. Human tissue was acquired from patients undergoing routine surgery at the Queen Elizabeth University Hospital (QEUH), Glasgow, UK. Tissue was collected by the Greater Glasgow and Clyde Biorepository on our behalf. The tissue consisted of subcutaneous fat from the breast or abdomen of female patients between the ages of 20 and 60 years old. Tissue was only taken from patients not receiving ongoing cancer treatment.

Tissue culture. Human subcutaneous fat was stored in Aqix (Life Science Production, UK) prior to culture. Under aseptic conditions, small pieces of tissue (3–5 mm²) were dissected and 4 pieces placed in each well of a 12 well plate. Matrigel (400 µl; Corning, NY, USA) was then added to each well and the plate was incubated at 37 °C for 30 minutes to polymerise the Matrigel. The wells were then supplemented with 2 ml of endothelial growth medium (EGM) (Promocell, Germany). The plates were incubated at 37 °C in 5% CO₂. Media was replaced every three days.

Ear implant surgery. After 7 days of culture, tissue with more than 0.25 mm of external inosculation around the entire outer circumference was implanted into mice (Fig. 1e). All surgical procedures took place in a Category 2 biological safety cabinet under aseptic conditions. The mice were anaesthetised with oxygen (1.5 L/minute) containing 2.5% isoflurane and prophylactically treated with buprenorphine (0.1 mg/kg). The ear was cleaned with 70% alcohol. It was then affixed to double sided adhesive tape on the bore of a 5 ml syringe. The ear pinna was injected with 50–100 µl of sterile saline to create a pocket. Forceps were then inserted into the ear to create an incision, which was enlarged using microdissection scissors. Curved forceps were used to enlarge the pocket and separate the skin of the ear pinna. The Matrigel embedded tissue was then inserted into the pocket and the incision was sealed using Vetbond glue (3M, MN, USA). Mice were recovered with oxygen before being moved to an IVC placed on a heat mat for 1 hour. They were returned to normal housing and monitored daily until the implants had fully healed. All experiments were carried out using these mice 21–35 days post-surgery unless otherwise stated.

Flow cytometry. Comparisons of fresh, cultured and implanted tissues were performed using flow cytometry. The tissues were all processed using the same method with some minor changes. Prior to digestion, each well containing cultured tissue was incubated with 1 mg/ml dispase II (ThermoFisher, Waltham, MA, USA) in Ca²⁺/Mg²⁺ free PBS for 1 hour at 37 °C to dissolve the Matrigel. The tissues in these wells were analysed together and the results divided by the number of embedded pieces of tissue in the well. Engrafted mice were culled 21 days post-surgery and their implant and control ears removed and placed in RPMI prior to digestion. All other processing steps were identical between the different tissue conditions.

Once collected, the tissues were minced and digested in RPMI containing 2% foetal bovine serum (FBS) (ThermoFisher, Waltham, MA, USA), 1 mg/ml collagenase II ((Sigma Aldrich, Dorset, UK) and 10 U/ml DNase (Invitrogen, Carlsbad, CA, USA) for 50 minutes at 37 °C under constant agitation. The tissues were processed through a 100 µm filter and washed twice in 2% FBS RPMI and once in Ca²⁺/Mg²⁺ free PBS containing 2 mM EDTA at 400 g for 5 minutes. Blood was not digested. The cell solutions were then suspended in 400 µl Ca²⁺/Mg²⁺ free PBS containing eFluor 506 viability dye (1:1000) (eBiosciences, Waltham, MA, USA) and incubated for 20 minutes at 4 °C. This step was omitted in samples examining labelled infected red blood cells. The cells were washed in Ca²⁺/Mg²⁺ free PBS containing 2 mM EDTA and resuspended in conditioned media from the anti-CD16/CD32 antibody producing hybridoma (2.4G2) (FcBlock). To examine human endothelial cells, antibody suspensions containing human Fc Block, V450 labelled anti-human CD36 (both from BD Biosciences, San Jose, USA), APC-eFluor 780 labelled anti-human CD45, APC labelled anti-mouse CD31, PE labelled anti-human CD31, AF700 labelled anti-human CD34 (all from Biolegend, San Diego, CA, USA), PE-Cy7 labelled anti-mouse CD45 and PerCP-eFluor 710 labelled anti-human ICAM-1 (both from eBiosciences, Waltham, MA, USA) were added to each sample and incubated for 20 minutes at 4 °C. To examine labelled infected red blood cells *in vivo*, antibody suspensions were prepared using PE-Cy7 labelled anti-mouse CD45 as above, APC labelled anti-mouse Ter119 (from eBiosciences, Waltham, MA, USA) and, depending upon the experiment, PerCP-Cy5.5 labelled anti-human CD235a (from Biolegend, San Diego, CA, USA) and incubated as described above. The cells were

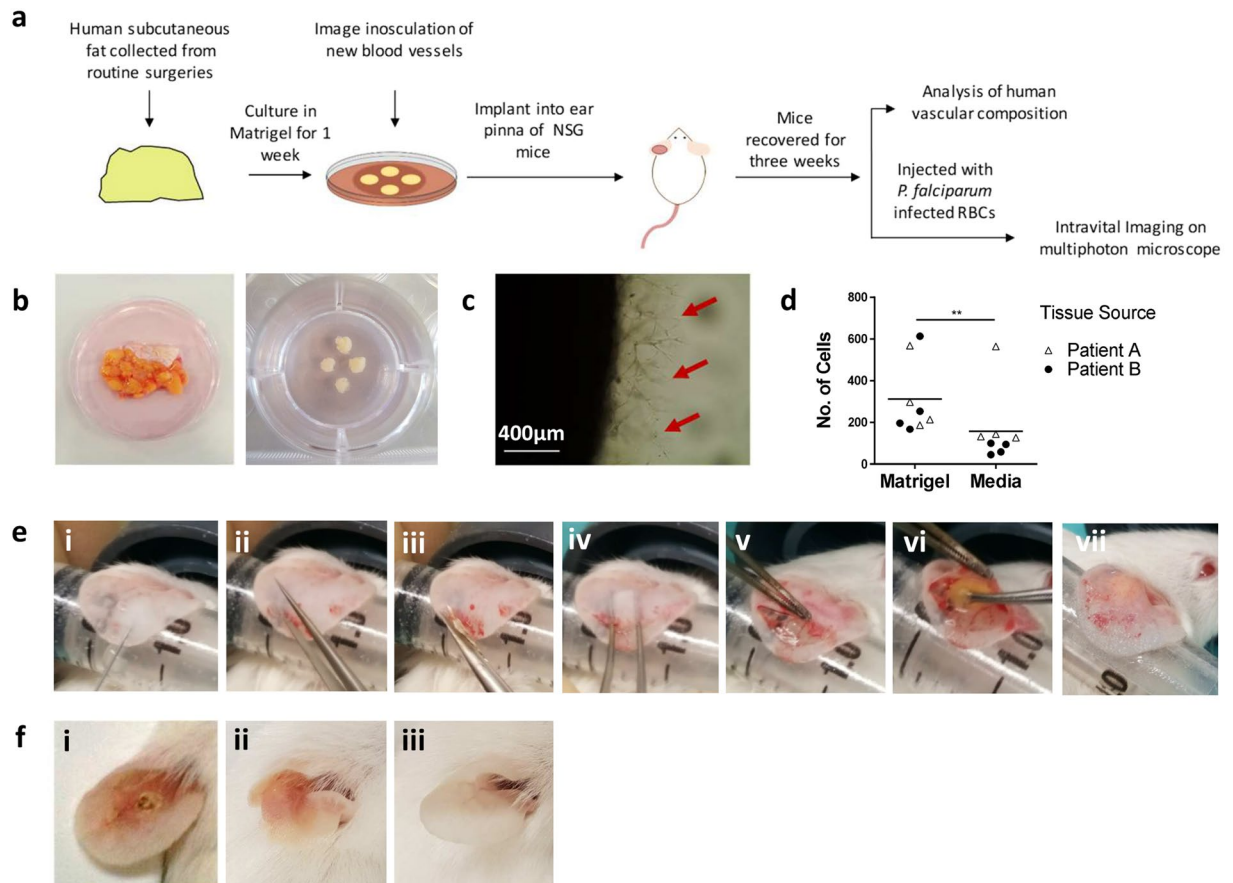


Figure 1. Developing a method for implanting human tissue into the ear pinna of immunocompromised mice. **(a)** Schematic of the model. **(b)** Human subcutaneous fat was collected from routine surgeries and dissected into 3–5mm² sized pieces before being embedded in Matrigel **(c)** which promoted the outgrowth of blood vessels (red arrows). **(d)** Comparisons of Matrigel embedded versus non Matrigel embedded tissues indicated an increase in the number of endothelial cells in embedded tissues. **(e)** The surgery was performed by **(i)** affixing the ear pinna to a syringe and injecting 50 μ l of saline to create a pocket. **(ii)** A hole was created using forceps. **(iii)** Scissors were inserted in this hole and used to create a flap. **(iv)** Curved forceps were used to split the skin apart to create a larger pocket. **(v)** The superior skin was retracted and **(vi)** the human tissue was inserted. **(vii)** The incision was sealed with glue and the mouse recovered. **(f,i)** Ears implanted with human tissue using a previous method²³ did not heal well. **(ii)** Ears implanted with tissue using the new method healed well three weeks post-surgery and resembled the **(iii)** control ear. **(d)** n = 8, pooled from two independent experiments. Statistical analysis was performed using a Mann Whitney test, **p < 0.01.

subsequently washed and analysed using a BD LSRfortessa flow cytometer (BD Biosciences, San Jose, USA). Analysis of flow cytometry data was performed using FlowJo 10 (FlowJo LLC, Ashland, OR, USA).

Histology. Mice were euthanized, and both the implant and controls ears were cut off and placed in 10% neutral buffered formalin for 16 hours. The tissue was then dehydrated through different grades of alcohol and xylene and embedded in wax. 8 μ m transverse sections were cut from each tissue and mounted on glass slides. They were then stained with haematoxylin and eosin and subsequently imaged on an EVOS Cell Imaging System (ThermoFisher, Waltham, MA, USA).

Immunofluorescence. Mice were euthanized, and both the implant and controls ears were cut off and placed in PBS. Using forceps, the skin on the ventral side of the ear was retracted to expose the human tissue implant. The ears were fixed in 4% paraformaldehyde for 20 minutes at 4 °C and incubated overnight in 0.05% Triton X-100 in PBS containing anti-human CD31 (Biolegend, San Diego, CA, USA) antibody conjugated to either PE or AF647 in a 1:200 dilution. The tissue was washed in PBS and mounted on a glass slide with a glass coverslip for imaging.

Parasites. *P. falciparum* was cultured as described previously^{16,17}. Cultures were grown in RPMI-1640 Supplemented with 24 mM sodium bicarbonate (Sigma-Aldrich, St Louis, MO, USA) and 10% human serum (Interstate Blood Bank Inc, Memphis, TN, USA). They were gassed with 5% CO₂/1% O₂ and 94% N₂ mixture and maintained at 37 °C. The ICAM-1/CD36 binding parasite strain ItG was used throughout¹⁸.

Parasites were magnetically purified using CS columns (Miltenyi-Biotech, Bergisch Gladbach, Germany) in a SuperMACS II separator (Miltenyi-Biotech, Bergisch Gladbach, Germany) as per manufacturer's instructions. Columns were blocked with 3% BSA for 15 minutes. One 50mm x 9mm petri dish containing 25 ml of parasites, maintained at 8–10% parasitaemia at a 5% haematocrit produced approximately 6×10^8 infected RBCs at a purity of 80–90%. The parasites were ready to use when in mid/late trophozoites stages. They were washed and resuspended in 20 ml of serum free RPMI and added to the column. Once the parasites had run through the column, it was washed with 25 ml of serum free RPMI. The column was detached from the magnet and the parasites were removed by washing with 50 ml of serum free RPMI.

Labelling red blood cells. Red blood cells (RBCs) with and without parasites were fluorescently labelled with CMTPX (ThermoFisher, Waltham, MA, USA). All labelling and incubation steps took place at 37 °C under constant agitation. RBCs were incubated with CMTPX (5 μ M) for 20 minutes. 1 ml of dye was used to stain 1×10^8 RBCs. Following staining, the RBCs were washed twice at x400 g for 5 minutes and incubated with 10% RPMI for 10 minutes. The RBCs were washed a further two times at x400 g for 5 minutes in $\text{Ca}^{2+}/\text{Mg}^{2+}$ free PBS and resuspended in 100 μ l of $\text{Ca}^{2+}/\text{Mg}^{2+}$ free PBS.

Static binding assay. On a marked plastic 60 mm \times 15 mm petri dish, 2 μ l drops of human ICAM-1 (R&D Systems, MN, USA), mouse ICAM-1 (R&D Systems, MN, USA) or PBS were added in triplicate around the sides of the dish. The dish was placed in a humidity chamber and incubated at 37 °C for 1 hour. The spots were then removed, and the dish was blocked in 1% BSA in PBS at 37 °C for 1 hour. A suspension of *P. falciparum* trophozoites at 3% parasitaemia in 1% haematocrit was prepared. 1.25 ml of parasite suspension was added to the dish, which was swirled occasionally, for 1 hour at 37 °C. The parasites were gently removed, and the dish was gently washed in RPMI 5 times. The bound parasites were then fixed in 1% glutaraldehyde in PBS at room temperature for 20 minutes. Imaging of the dish was performed using an EVOS Cell Imaging System (ThermoFisher, Waltham, MA, USA). One image was taken in the centre of each spot and the number of bound parasites was calculated.

Multiphoton imaging of implants. Multiphoton imaging was performed with a Zeiss LSM7 MP system equipped with both a 10x/0.3 NA air and a 20x/1.0NA water immersion objective lens (Zeiss) and a tuneable titanium/sapphire solid state 2-photon excitation source (Chameleon Ultra II; Coherent Laser Group) and optical parametric oscillator (OPO; Coherent Laser Group). For intravital imaging, mice were given an intravenous injection of 20 μ g of PE labelled or AF647 labelled anti-human CD31 and 5 μ g TNF α in PBS. Following six hours of incubation, the mice were injected intravenously with 5×10^8 uninfected unlabelled RBCs and anaesthetised with oxygen (1.5 L/minute) containing 2.5% isoflurane. The implant or control ear was affixed to a metal stage using veterinary-grade glue (Vetbond; 3M). Silicone grease was used to create a ring around the ear, which was then filled with PBS (Supplementary Fig. 4). When under the microscope, mice were given an injection of 5×10^8 CMTPX labelled infected red blood cells in the tail vein. A laser output of 820 nm with or without an OPO signal at 1060 nm provided excitation of adipocytes, hCD31 positive cells and labelled red blood cells. Images were acquired with an X-Y pixel resolution of 512 \times 512 in a variety of Z increments. For vessel analysis, 5 \times 5 tile scans of 100 μ m stacks were acquired in 4 μ m Z stack increments. All images were processed using Volocity 6.1.1 (Perkin Elmer, Cambridge, UK).

Image analysis. Analysis of human blood vessels was performed using images of fresh and implanted human tissue from different patients. Between 2 and 3 animals implanted with the same human tissue were used per data point for the implanted images. All images were analysed using the Vessel Analysis plugin provided by Fiji. Z stacks were first flattened then converted to binary images. The vascular density plugin was then run to produce the vascular density and vascular length density measurements. Vessel diameters were measured manually by counting five randomly selected vessels in five fields of view in each image.

Analysis of infected RBCs *in vivo* was performed using Imaris Version 7.6.5. Individual cells were defined as objects and tracked in 2D. Track plots demonstrate the movement of cells relative to their point of origin in the blood vessels.

Statistical analysis. All graphs and statistical analyses were produced using GraphPad Prism 7 (GraphPad Software Inc., San Diego, CA, USA). P values < 0.05 were deemed to be significant.

Results

Developing a method for implanting human tissue into the ear pinna. The basic layout of the xenograft model is shown in Fig. 1a. We focussed specifically on subcutaneous adipose tissue (SAT) for development of the model as it is well vascularised and is an important site in both infection and immunity^{19,20}. The tissue is also a common by-product of surgery and was therefore readily available for technical optimisation. Although not characterised as fully as SAT, we also had limited success implanting dermis, kidney cortex and skeletal muscle into the ear pinna as shown from histology studies of the tissues three weeks post-implantation. However, we were unable to form stable grafts consisting of brain, duodenum or colon as these tissues underwent major morphological changes upon implantation (Fig. S1).

Initial work examined whether tissue could be implanted directly from patients into the ear pinna of mice. We found that these tissues healed poorly and lost a substantial proportion of graft vasculature (data not shown). We therefore decided to culture the human tissue prior to implantation to stimulate the outgrowth of blood vessels²¹. To achieve this, tissues were embedded in Matrigel supplemented with endothelial growth medium (Fig. 1b). Consistent with previous studies²², this improved the retention of vessels of graft origin (Fig. 1c). Flow cytometric

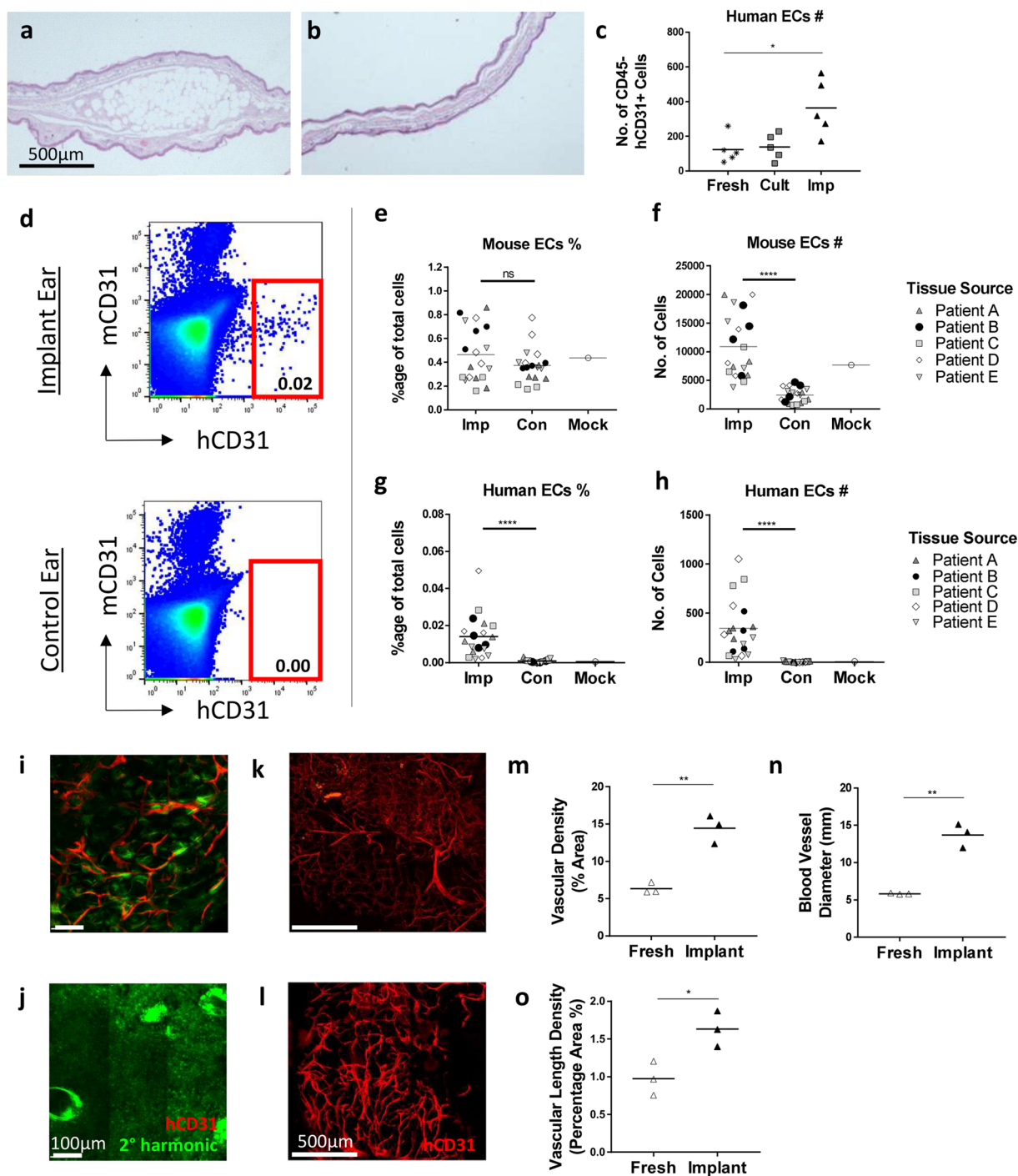


Figure 2. Human vasculature is retained in engrafted tissue. Analysis was performed on fresh, cultured and implanted human tissue to determine the effect of engraftment. Histological staining of the (a) implant and (b) control ear demonstrated that the human tissue survived implantation. (c) Flow cytometry was performed to determine the endothelial cell (EC) content of fresh, cultured (Cult) and implanted (Imp) tissue. $n = 5$ from five independent experiments. Each data point from implanted samples was pooled from 3–4 mice implanted with human tissue from the same source. Statistical analysis was performed using a Kruskal-Wallis test, $*p < 0.05$. (d–h) Flow cytometry was performed on implant (Imp), mock surgery (Mock) and control (Con) ears to examine the mouse and human ECs populations. 3–4 mice per group, five independent experiments. Statistical analysis was performed using a Wilcoxon test, $****p < 0.0001$. (i) An intravenous injection of an anti-human CD31 antibody confirmed that the engrafted tissue contained human ECs and was perfused. (j) The control ear confirmed that the antibody was human specific. Tile scans were taken of (k) fresh and (l) implanted human tissue stained with an anti-human CD31 antibody. Images were centred on the core of the tissues but included most vessels on the periphery. The changes in the blood vessels were quantitatively measured using a Fiji plugin called Vessel Analysis which determined the (m) vascular density, and (n) vascular length density. Blood vessel diameters (o) were measured manually by counting five randomly selected blood vessels in five fields of view in

each image. $n = 3$ from three independent experiments. Each data point from implanted samples was pooled from 2–3 mice implanted with human tissue from the same source. Statistical analysis was performed using an unpaired T test, * $p < 0.05$, ** $p < 0.01$.

analysis of engrafted implants indicated that a significantly higher number of human ECs (Mann-Whitney, $P < 0.01$) were found in Matrigel embedded tissues compared to those cultured without Matrigel (Fig. 1d). This confirmed that the pre-treatment improved the retention of the human vasculature in grafts, as shown in previous animal engraftment studies²².

Following 7 days of culture, tissues with externally inoculated vessels at least 0.15 mm in length around their entire outer circumference were implanted into NSG mice. Our previously described implantation method²³ resulted in poor wound healing with human tissue (Fig. 1fi). We therefore optimised the surgical approach by creating a large pocket in the mouse ear pinna (Fig. 1e). To achieve this, sterile saline was first injected into the ear pinna to create a subcutaneous pouch (i). Forceps were then placed into the needle entry site to enlarge the opening (ii) and an incision was made using scissors (iii). Curved forceps were then used to expand the pouch and separate the skin (iv). The skin on the ventral side was retracted (v) and Matrigel embedded SAT was placed within the pouch (vi). Finally, the incision was sealed using veterinary grade glue (vii). Following three weeks of recovery, the ear pinna had fully healed (Fig. 1fii) and resembled the control ear (Fig. 1fiii) confirming that tissue could be successfully engrafted using this method.

Human tissue survives and retains human vasculature following implantation into the ear pinna of immunocompromised mice.

Having developed a method for implanting human tissue into the ear pinna, we next had to determine whether the grafts survived and retained human vasculature. Histological analysis of implant (Fig. 2a) and control (Fig. 2b) ears demonstrated that the adipocytes and stroma of the transplanted tissue retained their normal structural characteristics and did not form a necrotic core. The grafts survived for up to five weeks post-implantation but may survive longer as has been shown in previous human engraftment studies^{4,5}. Flow cytometry analysis was performed to identify transplant ECs (mouse CD45–(mCD45)/human CD45–(hCD45), mouse CD31–(mCD31)/human CD31+(hCD31)) in the fresh, cultured and implanted human SAT (Fig. S2). Examination of the total number of human ECs indicated that the implants contained a significantly higher number of ECs than the fresh tissues (Fig. 2c) (Kruskal-Wallis test, $P < 0.05$). A breakdown of the EC subpopulations indicated few changes in the proportions of ECs expressing the adhesion molecules CD34 (Fig. S3A) and ICAM-1 (Fig. S3B) suggesting that the cells had not become activated as a result of implantation. However, the percentage of ECs expressing the scavenger marker CD36 (Fig. S3C) was significantly lower in implanted tissue suggesting a transplant induced reduction in the subcutaneous microvasculature characteristics of the tissue²⁴ (Two-Way ANOVA, $P < 0.0001$).

Flow cytometry of control, mock surgery (surgery with no tissue implants) and implant ears indicated the presence of human ECs in the implant ears only (Fig. 2d). The percentage of mouse ECs was not significantly different between treatments (Fig. 2e) but the number of mouse ECs was significantly higher in the implant ear compared to the control ear (Fig. 2f) (Wilcoxon Test, $P < 0.0001$). The number of cells were similar to those observed in the mock surgery ear suggesting that the increase was related to healing in response to surgery. By contrast, the percentage (Fig. 2g) and number (Fig. 2h) of human ECs were found to be significantly increased in the implant ears compared to the control ears (Wilcoxon Test, $P < 0.0001$) and were completely absent in the mock surgery control. This confirmed that the human ECs had been retained and had expanded in the implant ear following surgery.

To definitively confirm that the tissues had successfully anastomosed with the recipient mouse vasculature, we intravenously injected engrafted mice with a human specific α CD31 antibody. After one hour, we culled the mouse and imaged the tissue using multiphoton microscopy. Analysis of these images clearly demonstrated that the implanted tissues contained human blood vessels (Fig. 2i) whereas no human vessels were detected in the mouse control ears (Fig. 2j).

Further analysis of the vasculature of hCD31 labelled fresh (Fig. 2k) and implanted (Fig. 2l) tissues indicated significantly higher vascular densities (Fig. 2m) and vascular length densities (Fig. 2o) in the implanted tissue (Unpaired T test, $P < 0.05$) particularly around the periphery of the graft (Fig. S4), as per previous engraftment research²⁵. Similarly, the blood vessel diameters (Fig. 2n) were also found to be significantly larger in the implanted tissue suggesting a reduction in the microvasculature as shown by flow cytometry (Fig. S3C). The human vasculature was present for up to five weeks in our study. Although we did not examine later time points we would expect it to survive longer as shown with previous human EC engraftment studies²⁶.

Tracking labelled red blood cells *in vivo*. To image the intravascular behaviours of *P. falciparum* to human endothelium, we selected an ICAM-1 binding parasite known as ItG¹⁸. From our flow cytometry data (Fig. S3B) we knew that ICAM-1 was widely expressed on the human ECs and that this expression of this receptor could be increased by pre-treatment with TNF α (Fig. 3a). Using *in vitro* static binding assays, we confirmed that the parasite specifically bound to human recombinant ICAM-1 and not the mouse homologue (Fig. 3b), confirming that the parasite would only bind to human endothelium and was therefore suitable for our study.

Parasites were purified in the trophozoite stage of their lifecycle and labelled with the intracellular fluorescent dye, CMTPX (Fig. 3c). Following injection, we determined the circulation time of the parasite infected (iRBCs) and uninfected (uRBCs) red blood cells by taking regular blood samples over an hour and quantifying cell number by flow cytometry (Fig. 3d). This indicated that the parasites had a short circulation time, being cleared from the blood entirely within 20 minutes of the initial injection (Fig. 3e). However, we found that we could extend the

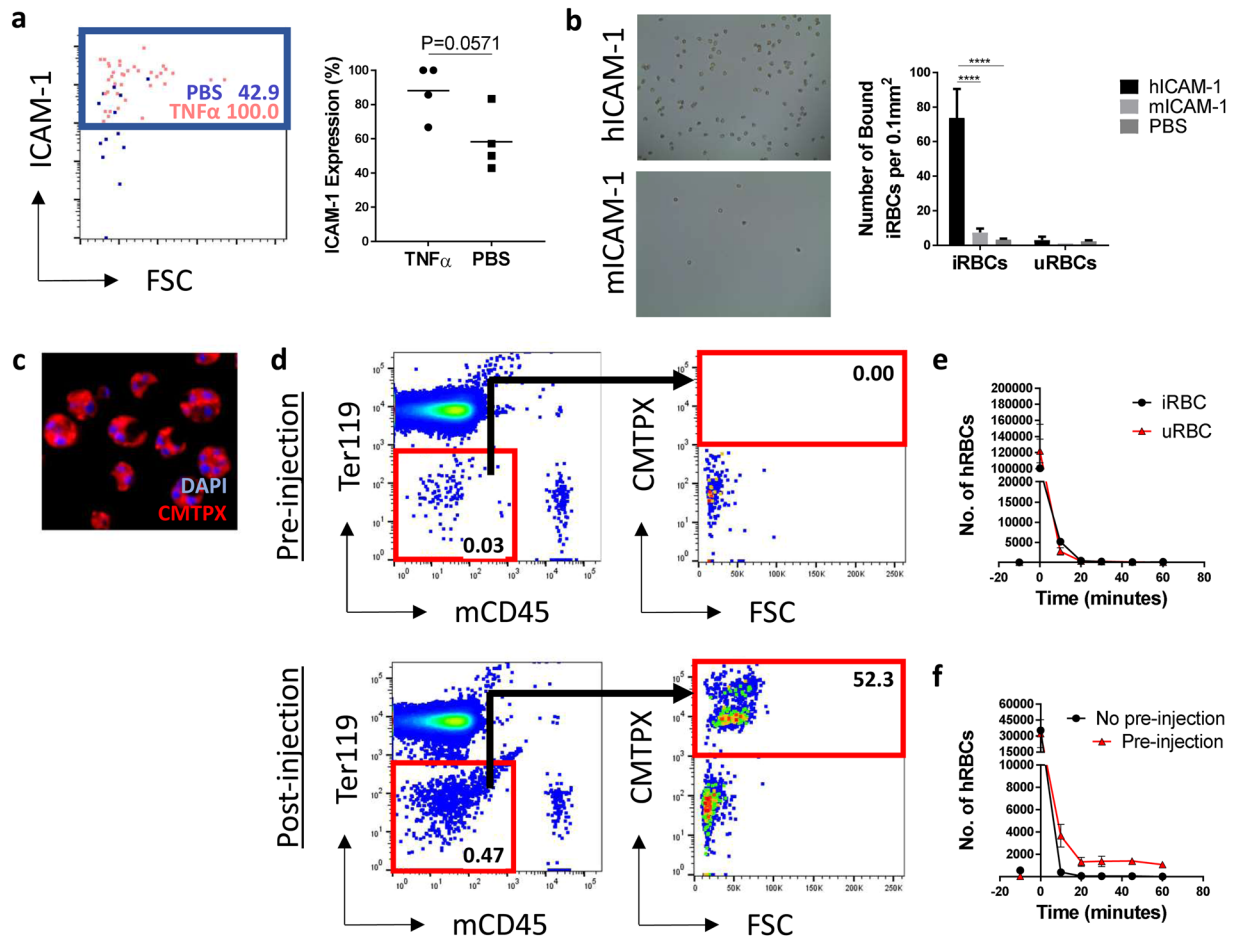


Figure 3. Tracking labelled red blood cells *in vivo*. (a) Human endothelial cell ICAM-1 expression was induced by intravenously injecting engrafted mice with human TNF α (5 μ g/mouse) 6 hours before they were culled. Control mice received PBS alone. n = 4, one independent experiment. Statistical analysis was performed using a Mann-Whitney test. *p < 0.05. (b) The *P. falciparum* parasite, ItG, was shown to bind specifically to human recombinant ICAM-1 using *in vitro* binding assays. n = 3, one independent experiment. Statistical analysis was performed using a Two-Way ANOVA with Tukey's multiple comparisons, ****p < 0.0001. (c) Infected and uninfected RBCs were labelled with CMTPX. (d–f) RBCs were injected intravenously into mice with human tissue implants and their depletion from the circulation was assessed by flow cytometry. The number of CMTPX labelled uninfected and infected RBCs was assessed without (e) and with (f) a pre-injection of unlabelled, uninfected RBCs. n = 4, one independent experiment.

circulation time of the labelled cells by giving a pre-injection of 5×10^9 unlabelled uRBCs to saturate the mouse macrophages that were responsible for removing the cells²⁷ (Fig. 3f). This allowed approximately 20,000 labelled RBCs to remain in the circulation throughout the imaging period allowing us to perform intravital imaging studies.

***P. falciparum* cytoadherence can be observed in human blood vessels.** After confirming that the *P. falciparum* parasite could bind to human ICAM-1 *in vitro*, we began intravital imaging studies (Fig. S5). Prior to imaging labelled RBCs, mice were pre-treated with unlabelled uRBCs to increase circulation time, TNF α to enhance ICAM-1 expression on transplants and finally a fluorescently labelled human anti-CD31 antibody to identify human blood vessels *in vivo*, following the protocols established above. Mice were then injected intravenously with labelled iRBCs and a multiphoton microscope was used to image the cells interacting with the labelled human vasculature. Several behaviours associated with cytoadherence were observed including cell tethering and rolling (Fig. 4a, Supplementary Video 1), adherence of iRBCs to blood vessel walls (Fig. 4b, Supplementary Video 2), blood vessel occlusion (Supplementary Video 2) and collections of iRBC around blood vessel junctions (Fig. 4c, Supplementary Video 3). An example of the analysis we could perform on the circulating iRBCs indicated differences in the speed of cells as they sequestered in blood vessels (Fig. 4d). Sequestration was confirmed to be specific to human blood vessels through flow cytometry (Figs. S6, 4e,f), which shown a significantly higher number of iRBCs in the implant ear compared to the control ear (Paired T Test, P < 0.05).

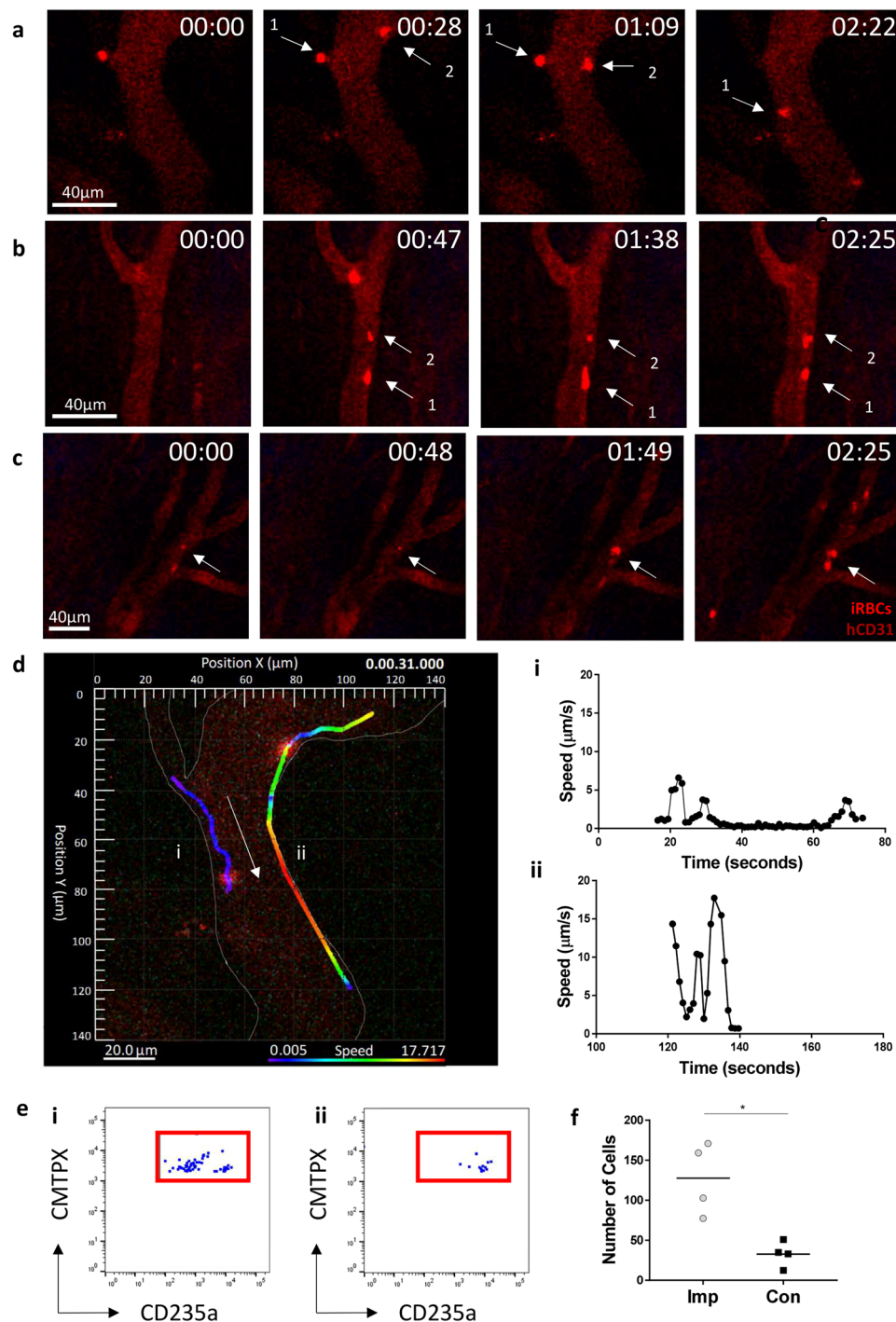


Figure 4. *P. falciparum* cytoadherence can be observed in human blood vessels. Intravital imaging was performed using a multiphoton microscope. Mice were pre-treated with $\text{TNF}\alpha$, unlabelled, uninfected RBCs, and AF647 labelled anti-human CD31 antibody. Labelled iRBCs were then injected into the tail vein of the mice. (a) Tethering and rolling (b) adherence of iRBCs to blood vessel walls (c) and collections of iRBCs around blood vessel junctions were all observed. $n = 3$, three independent experiments. (d) An example of imaging analysis indicated differences in the speed of sequestering cells over time in two different iRBCs (i & ii). Arrow indicates direction of blood flow. Rainbow bar indicates speed of iRBC in blood vessel. Flow cytometry was performed on the (e)(i) implant and (ii) control ears to compare the (f) number of iRBCs in the tissues. $n = 4$, from one independent experiment. Statistical analysis was performed using a paired T test, $*p < 0.05$.

Discussion

Here, we describe a novel method for culturing and implanting human tissue that promotes the retention and expansion of human vasculature. This system is potentially more biologically relevant than current animal xenograft models, allowing the study and direct observation of human vasculature *in vivo* and the interactions of cells

and molecules in vascular processes and diseases. As an example, we demonstrate the application of this approach to the study of *Plasmodium* parasites whose interactions with human vasculature are central to infection associated disease processes.

A key step in maintaining human vasculature in xenografts was to pre-culture tissue in an angiogenic extracellular matrix. This promoted the formation of capillary sprouts and the outgrowth of blood vessels prior to implantation²¹. Previous studies found that this significantly improved the retention of blood vessels of graft origin in murine allografts²², however, to the best of our knowledge, this is the first time this has been applied in human xenografts.

Alternative models which employ the use of human endothelial cells lines, such as human umbilical vein endothelial cells (HUVECs), to form microvascular networks have been used extensively to study blood vessel development *in vivo*²⁶ but have several drawbacks. These cell lines lack the heterogeneity of ECs and do not account for differences in cell phenotype, which vary greatly depending upon the cells local microenvironment, state of activation and exposure to soluble mediators²⁸. Furthermore, the cell lines often lack or have variable levels of many common EC markers including CD34, CD36 and von-Willebrand factor^{29,30} which limits their ability to model the vasculature in different tissues. Our model overcomes these problems by maintaining the grafts endogenous vasculature allowing it to more closely resemble human tissue in its natural state.

Once the grafts were perfused, we noticed few changes in vascularisation between tissues used at different time points post-implantation. This suggested that the vascularisation was physiological and was not persistent and unresolved as is observed with pathological vascularisation. In line with previous studies, the ECs in the grafts were shown to have few phenotypic changes following culture and implantation³¹. However, we did observe a decrease in CD36 expression in implanted tissue, a marker that is particularly enriched in the microvasculature of SAT³². The decrease in CD36 expression in the flow cytometry data, alongside the increased vascular diameters suggested a loss of microvasculature in the grafts. We hypothesise that this may be due to changes in the microvascular organisation around the periphery of the graft.

The choice of the ear pinna as an engraftment site had several benefits over other imaging methods, particularly imaging windows³³. As the ear could be imaged without surgical exposure, we were able to perform intravital imaging of the mice over an extended period of time. This not only reduced the stress that the animal was under but also allowed for the same engrafted animal to be imaged repeatedly, resulting in a significant reduction in the number of animals required for experiments.

Using this method, we chose to examine cytoadherence of the human malarial parasite *P. falciparum* to human endothelium. This is a process that cannot be observed in murine *Plasmodium* infections due to the specific properties of the human-infective parasite³⁴. Using our model, we were able to observe the behaviours associated with cytoadherence including rolling, adherence and vessel occlusion³⁵. The ItG parasite used in this study was panned on ICAM-1 but was also capable of binding to CD36. As mentioned CD36 expression was downregulated in our ECs following implantation, which may have interfered with the ability of the parasites to sequester in the blood vessels. However, the level of ligand expression on the EC surface required for cytoadherence is unclear. Furthermore, although CD36 is the major adherence receptor in experimental cerebral malaria, it is not clinically significant in the human form of the disease as the adhesion protein on the surface of iRBCs, PfEMP-1, is capable of binding to a large number of receptors and is most associated with endothelial protein C receptor (EPCR)³⁶. This suggests that the impact of reduced CD36 expression would be minimal for studying other parasite strains using this model.

Previous xenograft models^{37,38} have utilised skin in *P. falciparum* research, however, this tissue is not recognised as a particularly significant site of parasite sequestration and cytoadherence^{39,40}. By contrast, blood vessels in SAT are a more prominent site of parasite sequestration and previous studies have investigated this tissue as a model to study molecular processes leading to cytoadherence in brain vasculature⁴¹. For these reasons, we focussed on transplantation of human SAT, however, a range of other tissues were also found to be compatible with the culturing and implantation method. The only tissues we were unable to successfully engraft were those that came from the digestive tract or brain. The ability to transplant a variety of tissues, including SAT, therefore makes our current approach more flexible and better suited to studying the molecular processes of parasite cytoadherence *in vivo*.

It is notoriously difficult to reconstitute human RBCs in mice due to their rapid removal from the circulation by splenic macrophages²⁷. In our model, we overcame this issue by giving the mice a pre-injection of uRBCs to saturate the macrophages, allowing us to extend the imaging window for our intravital work. An alternative method would have been to deplete the macrophages in advance using clodronate liposomes⁴²; however, due to the severely immunocompromised state of our mice we decided against this method due to welfare concerns.

Although this imaging work is preliminary, the model holds great potential in further assessing the behaviours of parasites, including *P. falciparum*, trypanosomes and schistosomes, as well as bacterial infections such as *Neisseria meningitidis*, which are all known to mediate effects in both the skin and adipose tissue in patients^{13,43}. Aside from infection research, the model could also be further adapted to include components of a human immune system, either through the transfer of peripheral blood mononuclear cells (PBMCs) or the transplantation of haematopoietic stem cells, which is a feature often incorporated into humanised models⁴⁴. This would allow us to visualise various aspects of immune cell behaviours, including extravasation, in real time using acute models of inflammation. Other applications in which a model of human vasculature would also be useful include diagnostic imaging in cardiovascular research⁴⁵ and drug screening in cancer studies¹².

In summary, we have developed a humanised xenograft model in the ear pinna of immunocompromised mice. This model retains the tissues endogenous human vasculature allowing for non-invasive longitudinal imaging of blood flow and cellular recruitment in a system that can be easily adapted to study a variety of different biological processes.

Data availability

The datasets generated during and/or analysed during the current study are available from the corresponding author on reasonable request.

Received: 25 April 2019; Accepted: 14 January 2020;

Published online: 06 February 2020

References

- Morton, J. J., Bird, G., Refaeli, Y. & Jimeno, A. Humanized Mouse Xenograft Models: Narrowing the Tumor – Microenvironment Gap. *Cancer Res.* **76**, 6153–6159 (2016).
- Yong, K., Her, Z. & Chen, Q. Humanized Mice as Unique Tools for Human-Specific Studies. *Arch. Immunol. Ther. Exp. (Warsz)*. **66**, 245–266 (2018).
- Shultz, L. D., Brehm, M. A., Garcia-martinez, J. V. & Greiner, D. L. Humanized mice for immune system investigation: progress, promise and challenges. *Nat. Publ. Gr.* **12**, 786–798 (2012).
- Saunders, M. C., Keller, J. T., Dunsker, S. B. & Mayfield, F. H. Survival of autologous fat grafts in humans and in mice. *Connect Tissue Res.* **8**, 85–91 (1981).
- Geens, M. *et al.* Spermatogonial survival after grafting human testicular tissue to immunodeficient mice. **21**, 390–396 (2006).
- Holen, I., Speirs, V., Morrissey, B. & Blyth, K. *In vivo* models in breast cancer research: progress, challenges and future directions. *Dis. Model. Mech.* **10**, 359–371 (2017).
- Mansour, A. A. *et al.* An *in vivo* model of functional and vascularized human brain organoids. *Nat. Biotechnol.* **36**, 432–441 (2018).
- Colton, C. K. Implantable biohybrid artificial organs. *Cell Transplant.* **4**, 415–436 (1995).
- Stein, I., Neeman, M., Shweiki, D., Itan, A. & Keshet, E. Stabilization of vascular endothelial growth factor mRNA by hypoxia and hypoglycemia and coregulation with other ischemia- induced genes. *Mol. Cell. Biol.* **15**, 5363–5368 (1995).
- Calcagni, M. *et al.* *In vivo* visualization of the origination of skin graft vasculature in a wild-type/GFP crossover model. *Microvasc. Res.* **82**, 237–245 (2011).
- Hylander, B. L. *et al.* Origin of the vasculature supporting growth of primary patient tumor xenografts. *J. Transl. Med.* **11**, 1–14 (2013).
- Dong, Z. *et al.* Xenograft tumors vascularized with murine blood vessels may overestimate the effect of anti-tumor drugs: A pilot study. *PLoS One* **8**, 1–8 (2013).
- De Niz, M. *et al.* Intravital imaging of host-parasite interactions in skin and adipose tissues. *Cell. Microbiol.* (2019).
- Storm, J. & Craig, A. G. Pathogenesis of cerebral malaria — inflammation and cytoadherence MALARIA. *Front. Cell. Infect. Microbiol.* **4**, 1–8 (2014).
- Ito, M. *et al.* NOD/SCID/yc null mouse: an excellent recipient mouse model for engraftment of human cells. *Blood* **100**, 3175–3182 (2002).
- Madkhali, A. M. *et al.* An Analysis of the Binding Characteristics of a Panel of Recently Selected ICAM-1 Binding Plasmodium falciparum Patient Isolates. *PLoS One* **9**, 4–11 (2014).
- Trager, W. & Jensen, J. Human Malaria parasites in continuous culture. *Science (80-.)*. **193**, 673–676 (1976).
- Ockenhouse, C. F. *et al.* Molecular Basis of Sequestration in Severe and Uncomplicated Plasmodium Falciparum Malaria: Differential Adhesion of Infected Erythrocytes to CD36 and ICAM-1. *J. Infect* **164**, 163–169 (1991).
- Desruisseaux, M. S., Nagajyothi, Trujillo, M. E., Tanowitz, H. B. & Scherer, P. E. Adipocyte, adipose tissue, and infectious disease. *Infect. Immun.* **75**, 1066–1078 (2007).
- Koethe, J. R., Hulgan, T. & Niswender, K. Adipose tissue and immune function: A review of evidence relevant to HIV infection. *J. Infect. Dis.* **208**, 1194–1201 (2013).
- Rojas-rodriguez, R. *et al.* Adipose Tissue Angiogenesis Assay. *Methods of Adipose Tissue Biology, Part A* **537**, (Elsevier Inc., 2014).
- Laschke, M. W. *et al.* Promoting external inosculation of prevascularised tissue constructs by pre-cultivation in an angiogenic extracellular matrix. *Eur. Cells Mater.* **20**, 356–366 (2010).
- Gibson, V. B. *et al.* A novel method to allow noninvasive, longitudinal imaging of the murine immune system *in vivo*. *Blood* **119**, 1–3 (2012).
- Swerlick, R. A., Lee, K. H., Wick, T. M. & Lawley, T. J. Human dermal microvascular endothelial but not human umbilical vein endothelial cells express CD36 *in vivo* and *in vitro*. *J. Immunol.* **148**, 78–83 (1992).
- Laschke, M. W. *et al.* Vascularisation of porous scaffolds is improved by incorporation of adipose tissue-derived microvascular fragments. *Eur. Cells Mater.* **24**, 266–277 (2012).
- Schechner, J. S. *et al.* *In vivo* formation of complex microvessels lined by human endothelial cells in an immunodeficient mouse. *PNAS* **97**, 9191–9196 (2000).
- Hu, Z., Rooijen, N. V. & Yang, Y. Macrophages prevent human red blood cell reconstitution in immunodeficient mice. *Blood* **118**, 5938–5946 (2012).
- Garlanda, C. & Dejana, E. Heterogeneity of Endothelial Cells. *Arterioscler. Thromb. Vasc. Biol.* **17**, 1193–1202 (1997).
- McCormick, C. J., Craig, A., Roberts, D., Newbold, C. I. & Berendt, A. R. Intercellular adhesion molecule-1 and CD36 synergize to mediate adherence of Plasmodium falciparum-infected erythrocytes to cultured human microvascular endothelial cells. *J. Clin. Invest.* **100**, 2521–2529 (1997).
- Müller, A. M. *et al.* Expression of the endothelial markers PECAM-1, vWF, and CD34 *in Vivo* and *in Vitro*. *Exp. Mol. Pathol.* **72**, 221–229 (2002).
- Motherwell, J. M., Anderson, C. R. & Murfee, W. L. Endothelial Cell Phenotypes are Maintained During Angiogenesis in Cultured Microvascular Networks. *Sci. Rep.* **8**, 1–11 (2018).
- Silverstein, R. L. & Febbraio, M. CD36, a Scavenger Receptor Involved in Immunity, Metabolism. *Angiogenesis, and Behavior. Sci. Signal.* **2**, 1–8 (2009).
- Laschke, M. W., Vollmar, B. & Menger, M. D. The dorsal skinfold chamber: Window into the dynamic interaction of biomaterials with their surrounding host tissue. *Eur. Cells Mater.* **22**, 147–167 (2011).
- Strangward, P. *et al.* A quantitative brain map of experimental cerebral malaria pathology. *PLoS Pathog.* **13**, 1–37 (2017).
- Helms, G., Dasanna, A. K., Schwarz, U. S. & Lanzer, M. Modeling cytoadhesion of Plasmodium falciparum-infected erythrocytes and leukocytes—common principles and distinctive features. *FEBS Lett.* 1955–1971 <https://doi.org/10.1002/1873-3468.12142> (2016).
- Mkumbaye, S. I. *et al.* The Severity of Plasmodium falciparum Infection Is Associated with Transcript Levels of var Genes Encoding Endothelial Protein C Receptor-Binding P. falciparum Erythrocyte Membrane Protein 1. *Cell. Microbiol.* **85**, 1–14 (2017).
- Ho, M., Hickey, M. J., Murray, A. G., Andonegui, G. & Kubes, P. Visualization of Plasmodium falciparum–Endothelium Interactions in Human Microvasculature: Mimicry of Leukocyte Recruitment. *J. Exp. Med.* **192**, 1205–1212 (2000).
- Yipp, B. G. *et al.* Differential roles of CD36, ICAM-1, and p-selectin in Plasmodium falciparum cytoadherence *in vivo*. *Microcirculation* **14**, 593–602 (2007).
- Jervis, H. R., Sprinz, H., Johnson, A. J. & Wellde, A. T. Experimental Infection in With. *Am. J. Trop. Med. Hygiene* **21**, 382–386 (1972).

40. MacPherson, G. G., Warrell, M. J., White, N. J., Looareesuwan, S. & Warrell, D. A. Human cerebral malaria. A quantitative ultrastructural analysis of parasitized erythrocyte sequestration. *Am. J. Pathol.* **119**, 385–401 (1985).
41. Moxon, C. A. *et al.* Loss of endothelial protein C receptors links coagulation and inflammation to parasite sequestration in cerebral malaria in African children. *Blood* **122**, 842–852 (2013).
42. Amaladoss, A. *et al.* De Novo Generated Human Red Blood Cells in Humanized Mice Support Plasmodium falciparum Infection. *PLoS One* **10**, e0129825 (2015).
43. Bruneval, P., Duménil, G., Michea Veloso, P., Martin, T. & Melican, K. Adhesion of Neisseria meningitidis to Dermal Vessels Leads to Local Vascular Damage and Purpura in a Humanized Mouse Model. *PLoS Pathog.* **9**, e1003139 (2013).
44. Minkah, N. K., Schafer, C. & Kappe, S. H. I. Humanized Mouse Models for the Study of Human Malaria Parasite Biology, Pathogenesis, and immunity. *Front. Immunol.* **9** (2018).
45. Noonan, J. *et al.* In vivo multiplex molecular imaging of vascular inflammation using surface-enhanced Raman spectroscopy. *Theranostics* **8**, 6195–6209 (2018).

Acknowledgements

We acknowledge the assistance of both the Institute of Infection, Immunity and Inflammation Flow Core Facility, the Glasgow Imaging Facility and the Histology Research Service at the University of Glasgow. We also acknowledge the support of NHS Research Scotland (NRS) Greater Glasgow and Clyde Biorepository in acquiring and processing human tissue samples. In addition, we acknowledge Janet Storm for kindly providing a protocol for the static binding assay. This work was supported by the Wellcome Trust [095507].

Author contributions

G.R.M. designed the research, performed the experiments, constructed the figures, analysed the data and wrote the manuscript. H.E.S. provided technical assistance and contributed to experimental design. R.O. and M.D.N. provided technical assistance and provided input in Plasmodium experiments. J.C.L. designed the research and performed the initial experiments. M.M. provided assistance in experimental design. P.G., A.C. and J.M.B. designed the research and contributed to writing the paper.

Competing interests

The authors declare no competing interests.

Additional information

Supplementary information is available for this paper at <https://doi.org/10.1038/s41598-020-58650-y>.

Correspondence and requests for materials should be addressed to J.M.B.

Reprints and permissions information is available at www.nature.com/reprints.

Publisher's note Springer Nature remains neutral with regard to jurisdictional claims in published maps and institutional affiliations.



Open Access This article is licensed under a Creative Commons Attribution 4.0 International License, which permits use, sharing, adaptation, distribution and reproduction in any medium or format, as long as you give appropriate credit to the original author(s) and the source, provide a link to the Creative Commons license, and indicate if changes were made. The images or other third party material in this article are included in the article's Creative Commons license, unless indicated otherwise in a credit line to the material. If material is not included in the article's Creative Commons license and your intended use is not permitted by statutory regulation or exceeds the permitted use, you will need to obtain permission directly from the copyright holder. To view a copy of this license, visit <http://creativecommons.org/licenses/by/4.0/>.

© The Author(s) 2020